crystals

MDPI

Article

Rare Earth Ion-Doped $Y_{2.95}R_{0.05}MgAl_3SiO_{12}$ (R = Yb, Y, Dy, Eu, Sm) Garnet-Type Microwave Ceramics for 5G Application

Zijun Ye [1], Yu Jiang [1], Minmin Mao [1,*], Zhiyu Xiu [1], Mengjiao Chi [1], Guofa Wu [1], Bing Liu [1], Dawei Wang [2,*], Bin Yang [3] and Kaixin Song [1,*]

1 College of Electronics Information, Hangzhou Dianzi University, Hangzhou 310018, China
2 Functional Materials and Acousto-Optic Instruments Institute, School of Instrumentation Science and Engineering, Harbin Institute of Technology, Harbin 150080, China
3 Faculty of Science and Engineering, University of Chester, Chester CH1 4BJ, UK
* Correspondence: mmm@hdu.edu.cn (M.M.); wangdawei102@gmail.com (D.W.); kxsong@hdu.edu.cn (K.S.)

Abstract: In this work, $Y_{2.95}R_{0.05}MgAl_3SiO_{12}$ (R = Yb, Y, Dy, Eu, Sm) microwave single-phase dielectric ceramics were successfully prepared via a conventional ceramic sintering technology by doping a series of rare earth elements (Yb, Y, Dy, Eu, Sm) with different ionic radii for the first time. The effects of A-sites occupied by rare earth elements on the microwave dielectric properties of $Y_{2.95}R_{0.05}MgAl_3SiO_{12}$ were studied using crystal structure refinement, a scanning electron microscope (SEM), bond valence theory, P-V-L theory, and infrared reflection spectroscopy. It was found that the ionicity of the Y-O bond, the lattice energy, the bond energy, and the bond valance of the $Al_{(Tet)}$-O bond had important effects on the microwave dielectric properties. Particularly, the optimum microwave dielectric properties, ε_r = 9.68, $Q \times f$ = 68,866 GHz, and τ_f = −35.8 ppm/°C, were obtained for $Y_{2.95}Dy_{0.05}MgAl_3SiO_{12}$ when sintered at 1575 °C for 6 h, displaying its potential for 5G communication.

Keywords: garnet; microwave dielectric properties; P–V–L theory; infrared reflection spectroscopy

check for updates

Citation: Ye, Z.; Jiang, Y.; Mao, M.; Xiu, Z.; Chi, M.; Wu, G.; Liu, B.; Wang, D.; Yang, B.; Song, K. Rare Earth Ion-Doped $Y_{2.95}R_{0.05}MgAl_3SiO_{12}$ (R = Yb, Y, Dy, Eu, Sm) Garnet-Type Microwave Ceramics for 5G Application. *Crystals* **2022**, *12*, 1608. https://doi.org/10.3390/cryst12111608

Academic Editor: Alessandro Chiasera

Received: 13 October 2022
Accepted: 7 November 2022
Published: 11 November 2022

1. Introduction

With the rapid development of communication frequency bands to millimeter-wave bands, the microwave dielectric ceramic materials used in communication equipment are required to include the following dielectric properties:

(1) low ε_r to reduce delay in the signal transmission process; (2) ultra-high $Q \times f$ values to reduce the transmission loss; (3) near-zero temperature coefficients (τ_f), which can improve the device stability in different environments when applied in resonators, antennas, filters, 5G base stations, etc. [1–6].

In low dielectric constant material systems, the $Y_3Al_5O_{12}$ garnet has attracted extensive research due to its low ε_r and high $Q \times f$ value in 5G communication systems [7]. Figure 1 shows the $Q \times f$ values of the various types of garnet-type microwave dielectric ceramics, including the vanadate garnet, aluminate garnet, etc. [8–24]. It is clear that the $Q \times f$ value of the aluminate garnet is much higher than that of others. The aluminate garnet has the formula of $Y_3Al_5O_{12}$ (YAG), in which three Y^{3+} ions occupy the dodecahedral A-site, two $Al_{(Oct)}{}^{3+}$ ions occupy the octahedral B-site, and three $Al_{(Tet)}{}^{3+}$ ions occupy the tetrahedral C-site. The $Q \times f$ value of $Y_3Al_5O_{12}$ microwave ceramics was initially reported to be as high as 440,000 GHz [25]. Later, Jin et al. [12] reported the excellent microwave dielectric properties of ε_r = 10.8, $Q \times f$ = 213,400 GHz, and τ_f = −30 ppm/°C for $Y_3Al_5O_{12}$ ceramics pressed under 200MPa by a cold isostatic pressing technology and sintered at 1750 °C for 5 h in a vacuum environment. Zhou et al. [15] synthesized $Y_3Al_{4.97}Mg_{0.03}O_{11.985}$ microwave ceramics by replacing $Al_{(Oct)}{}^{3+}$ with Mg^{2+} and sintering at 1700 °C for 12 h, which showed the following excellent microwave dielectric properties: ε_r = 10.9, $Q \times f$ = 218,168 GHz,

and τ_f = −30 ppm/°C. Then, non-stoichiometric YAG ceramics ($Y_{3.03}Al_5O_{12}$) were further synthesized at 1750 °C for 12 h, showing the following good microwave dielectric properties: ε_r = 11.2, $Q \times f$ = 236,936 GHz, and τ_f = −35.9 ppm/°C [16]. However, the sintering temperature of YAG ceramics was too high (>1700 °C), which does not conform to the concept of low carbon and environmental protection. In order to solve the problems of high-sintering temperatures and large τ_f values, much research has been carried out. Zhang et al. [14] reported that the sintering temperature of YAG ceramics was reduced from 1700 °C to 1360 °C by using LiF as an additive, producing properties of $Q \times f$ = 89,810 GHz, ε_r = 10.63, and τ_f = −51.4 ppm/°C. Peng et al. [26] reported a near-zero τ_f value (+7 ppm/°C) for Ca^{2+} and Ti^{4+} co-doped $Ca_{1.5}Y_{1.5}Al_{3.5}Ti_{1.5}O_{12}$ ceramics, as well as ε_r = 32.6 and $Q \times f$ = 45,200 GHz.

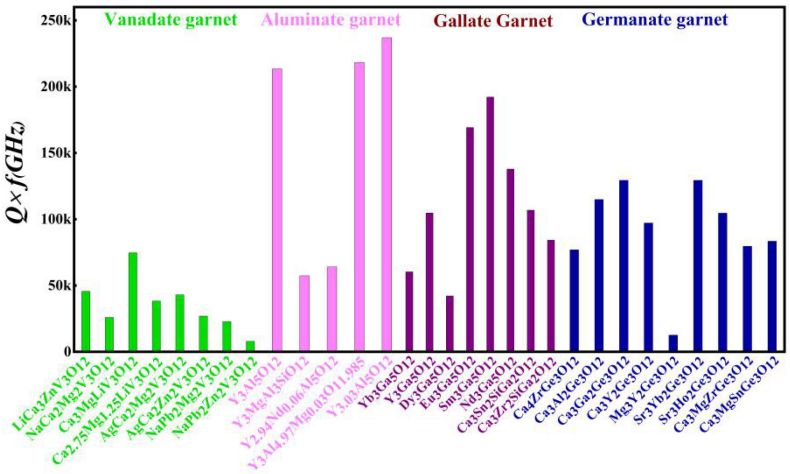

Figure 1. $Q \times f$ values of typical garnet-type microwave dielectric ceramics.

Previous reports have shown that a MgO-SiO_2 liquid phase was formed in $Y_3Al_5O_{12}$ garnet ceramics with MgO and SiO_2 as sintering aids, which improved the densification rate of the ceramics [27]. Compared with YAG ceramics, $Y_3MgAl_3SiO_{12}$ ceramics were formed by doping Mg^{2+} at the B-site octahedrons and Si^{4+} at the C-site tetrahedrons of YAG, which reduced the sintering temperature from 1670 °C to 1550 °C and exhibited the good microwave dielectric performances of ε_r = 10.1, $Q \times f$ = 57,340 GHz, and τ_f = −32 ppm/°C [13,28,29]. The τ_f of $Y_3MgAl_3SiO_{12}$ has been further tuned to a near-zero value (+5.2 ppm/°C) by forming composites with 0.2TiO_2 [30]. However, the modification of A-site dodecahedrons for garnet ceramics has been the subject of very little research. Herein, we have designed a scheme of A-site ionic substitution for the Y element in $Y_3MgAl_3SiO_{12}$ ceramics using a series of rare earth elements with different ionic radii (Yb, Y, Dy, Eu, Sm). The microwave dielectric properties of $Y_{2.95}R_{0.05}MgAl_3SiO_{12}$ (R = Yb, Y, Dy, Eu, Sm) ceramics were well discussed using crystal structure refinement, bond valence theory, P–V–L theory, and infrared reflectance spectrum.

2. Experimental Process

$Y_{2.95}R_{0.05}MgAl_3SiO_{12}$ (R = Yb, Y, Dy, Eu, Sm) ceramics were prepared using raw materials of Yb_2O_3 (Shanghai Aladdin Reagent Co., Ltd., Shanghai, China, 99.99%), Y_2O_3 (Shanghai Aladdin Reagent Co., Ltd., 99.99%), Dy_2O_3 (Shanghai Aladdin Reagent Co., Ltd., 99.99%), Eu_2O_3 (Shanghai Aladdin Reagent Co., Ltd., 99.99%), Sm_2O_3 (Shanghai Aladdin Reagent Co., Ltd., 99.99%), MgO (Shanghai Aladdin Reagent Co., Ltd., 99.99%), Al_2O_3 (Shanghai Aladdin Reagent Co., Ltd., 99.99%), and SiO_2 (Shanghai Aladdin Reagent Co., Ltd., 99.99%). Raw materials were weighed according to the stoichiometric ratio and planetarily ball-milled for 12 h in solvent ethanol. The speed for milling was 240 r/min. The mixed slurries were dried at 80 °C, and then the dried powders were calcined at 1400 °C for 4 h. The calcined powder was re-milled and mixed uniformly with 5 wt% organic

binders (polyvinyl alcohol). The granulated powder was sieved using a 60-mesh sieve and pressed into cylindrical green pellets with a diameter of 12 mm and a height of ~7 mm. The green pellets were first fired at 800 °C for 4 h to remove the binder and then sintered at 1500 °C–1650 °C for 6 h.

The crystal structure was identified by X-ray powder diffraction (XRD) (Shimadzu, Kyoto, Japan) using Cu Kα radiation at the range of 2θ from 10° to 80°, with a step size of 0.02°. The GSAS software was used to analyze the crystal structure parameters of XRD data [31,32]. The microstructure of the sintered samples was observed by a field emission scanning electron microscope (SEM, Sigma 300, ZEISS, Oberkochen, Germany). The Archimedes method was used to determine the bulk density. The infrared reflectance spectra were recorded using the Bruker IFS 66v beam line of the Hefei National Synchrotron Radiation Laboratory. Microwave dielectric properties were measured in $TE_{01\delta}$ mode using the resonant cavity method. The Keysight (N5234B) vector network analyzer was used for evaluating the Q × f values and ε_r. The τ_f value was calculated by the following formula [33]:

$$\tau_f = \frac{f_2 - f_1}{f_1 \times (T_2 - T_1)} \times 10^6 (\text{ ppm/°C}) \quad (1)$$

where f_1 and f_2 were the resonant frequency at 25 and 85 °C, respectively.

3. Results and Discussion

The XRD patterns of $Y_{2.95}R_{0.05}MgAl_3SiO_{12}$ (R = Yb, Y, Dy, Eu, Sm) ceramics are displayed in Figure 2. The diffraction peaks of all samples match well with the YAG structure (PDF No. 88-2047), indicating the formation of a garnet solid solution. It can be clearly seen that the diffraction peaks move to the lower 2θ angle with the increase in R ionic radius (Yb^{3+}—0.985 Å, Y^{3+}—1.019 Å, Dy^{3+}—1.027 Å, Eu^{3+}—1.066 Å, Sm^{3+}—1.079 Å) from magnified spectra in Figure 2b. The XRD data of the $Y_{2.95}R_{0.05}MgAl_3SiO_{12}$ ceramics, which are shown in Figure S2a–e, are analyzed using the Rietveld method. Table 1 lists the detailed refined parameters. Low Rietveld discrepancy factors (R_{wp}~9%, R_p~7%, χ^2~4) are obtained, suggesting that the refinement results are reliable. The unit cell volume of $Y_{2.95}R_{0.05}MgAl_3SiO_{12}$ ceramics increases slightly with increasing R ionic radius, which is consistent with the diffraction peak's shift toward the lower 2θ direction. The schematic crystal structure of $Y_{2.95}R_{0.05}MgAl_3SiO_{12}$ ceramics is given in Figure S1f.

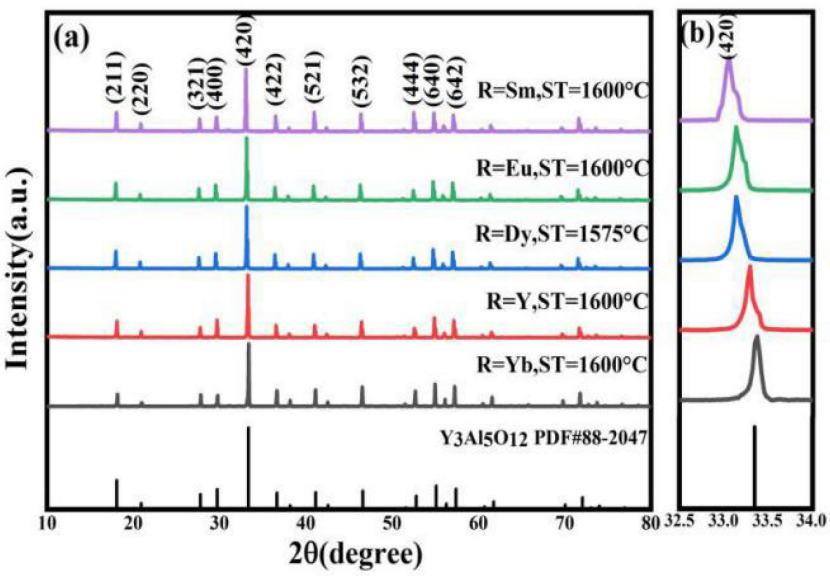

Figure 2. (**a**) XRD patterns of $Y_{2.95}R_{0.05}MgAl_3SiO_{12}$ (R = Yb, Y, Dy, Eu, Sm) ceramic samples; (**b**) magnified XRD spectra.

Table 1. The crystallographic data obtained by Rietveld refinement for $Y_{2.95}R_{0.05}MgAl_3SiO_{12}$ ceramics.

R	Yb	Y	Dy	Eu	Sm
Crystal system			cubic		
Space group			Ia-3d		
Z			8		
a = b = c(Å)	12.0482	12.0499	12.0529	12.0589	12.0668
α = β = γ(°)			90		
V_{cell}(Å^3)	1749.121	1749.607	1750.103	1750.623	1751.009
Calc.density(g/cm^3)	4.602	4.357	4.538	4.527	4.417
R_{wp}(%)	9.17	10.5	9.8	10.1	9.8
R_p(%)	6.34	7.38	8.37	8.87	6.5
χ^2	4.36	4.35	2.65	3.06	2.64
Y/R-O (Å)	2.2932	2.3224	2.3002	2.3106	2.3329
	2.4466	2.4770	2.4782	2.4796	2.4865
($Al_{(Oct)}$/Mg)-O (Å)	2.0038	1.9881	2.0062	1.9894	1.9649
($Al_{(Tet)}$/Si)-O (Å)	1.7355	1.7257	1.7352	1.7387	1.7528

The SEM images of the $Y_{2.95}R_{0.05}MgAl_3SiO_{12}$ (R = Yb, Y, Dy, Eu, Sm) ceramics sintered at the optimal sintering temperature (Yb—1600 °C, Y—1600 °C, Dy—1575 °C, Eu—1600 °C, Sm—1600 °C) are shown in Figure 3a–e. All sintered ceramics are dense except for the Sm-doped sample, which has obvious voids. The grain size distribution of each sample is shown in Figure S2 (Supplementary Materials), and the average grain size is plotted in Figure 3f. Among all samples in this study, $Y_{2.95}Dy_{0.05}MgAl_3SiO_{12}$ ceramic has the largest average grain size, indicating that Dy^{3+}-doping could be conducive to the densification and growth of ceramics.

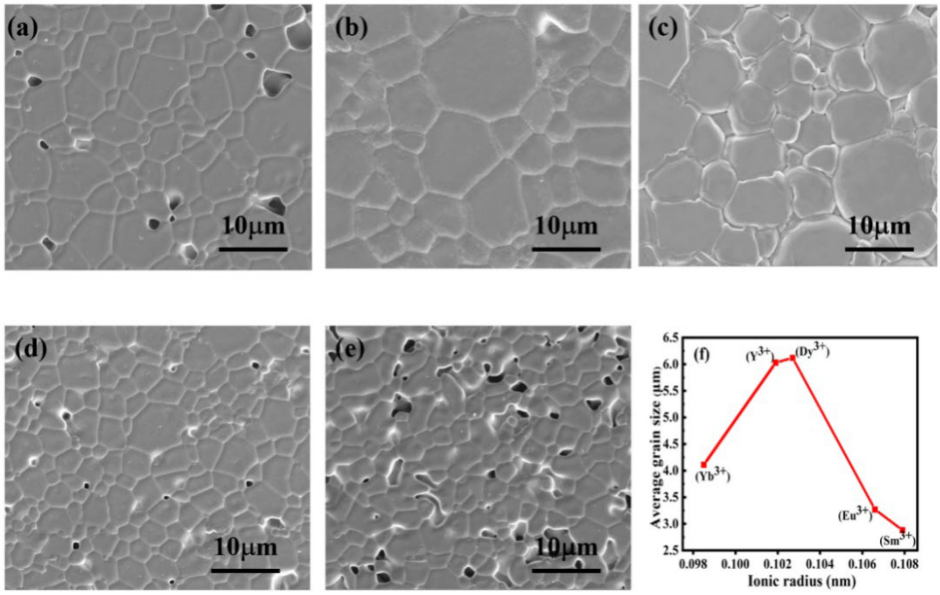

Figure 3. SEM images of $Y_{2.95}R_{0.05}MgAl_3SiO_{12}$ ceramics: (**a**) Yb; (**b**) Y; (**c**) Dy; (**d**) Eu; (**e**) Sm; (**f**) the average grain size as a function of ionic radius.

Figure 4 exhibits the microwave dielectric properties of $Y_{2.95}R_{0.05}MgAl_3SiO_{12}$ (R = Yb, Y, Dy, Eu, Sm) ceramics sintered at the optimal temperature. The ε_r values show a gradually increasing trend, except for Dy, which has a lower ε_r value of 9.68. The $Q \times f$ values are in the range of 47,000 GHz ~ 70,000 GHz, which is consistent with the trend of relative density (ρ_r). The τ_f value is between −38.7 ppm/°C and −28.6 ppm/°C. It is widely known that the microwave dielectric properties are dependent on both extrinsic (second phase, density, grain size, etc.) and intrinsic (lattice vibration) factors [34]. The relative densities

of $Y_{2.95}R_{0.05}MgAl_3SiO_{12}$ ceramics sintered at the optimal sintering temperature are high (ρ_r > 94%), and no secondary phases could be detected. Therefore, the intrinsic factors, such as the crystal structure and chemical bonds, played a decisive role in the dielectric properties. Herein, the relationship between the microwave dielectric properties and internal factors of the $Y_{2.95}R_{0.05}MgAl_3SiO_{12}$ ceramics is discussed using the P–V–L theory. The detailed calculation methods are included in the Supplementary Materials [35–38].

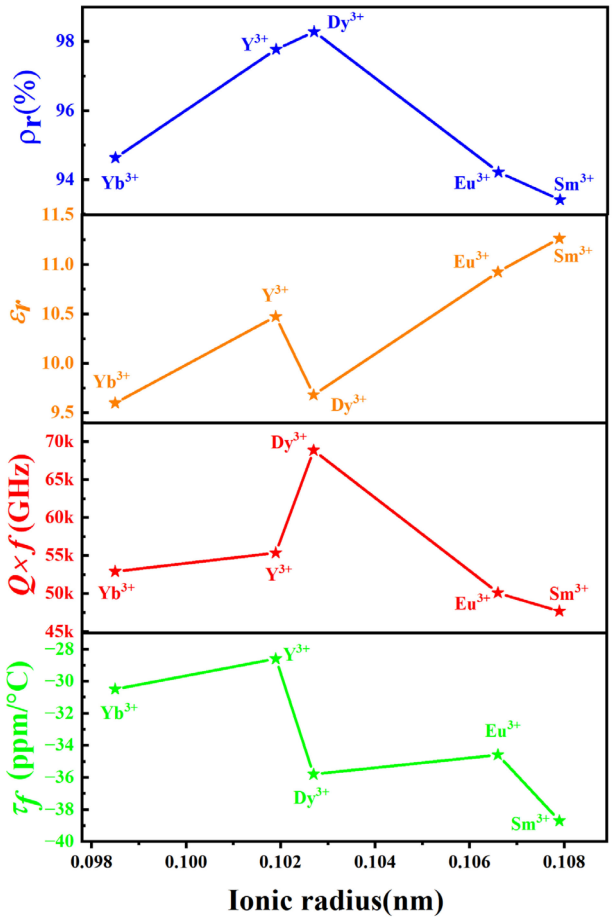

Figure 4. Microwave dielectric properties and ρ_r of $Y_{2.95}R_{0.05}MgAl_3SiO_{12}$ ceramics.

In general, the measured permittivity (ε_r) is related to the bond ionicity (f_i). The calculated results of f_i are listed in Table S1 (Supplementary Materials). In addition, the theoretical permittivity (ε_{theo}) of $Y_{2.95}R_{0.05}MgAl_3SiO_{12}$ ceramics can be calculated using the Clausius-Mosotti Equations (2) and (3) [39,40]:

$$\varepsilon_{theo} = \frac{3}{1 - b\alpha/V_m} - 2 \quad (2)$$

$$V_m = \frac{V_{cell}}{Z} \quad (3)$$

Moreover, the corrected dielectric constant (ε_c) by porosity (P) can be calculated by Equations (5) and (6) [41]:

$$\mathrm{P} = 1 - \rho_r \quad (4)$$

$$\varepsilon_c = \varepsilon_r(1 + 1.5\mathrm{P}) \quad (5)$$

As shown in Figure 5a, the ε_r is consistent with the changing trend of ε_{theo}, ε_c, and the average bond ionicity (Δf_i). The average ionicity properties of the Y-O, $Al_{(Oct)}$-O, and

$Al_{(Tet)}$-O bonds of $Y_{2.95}R_{0.05}MgAl_3SiO_{12}$ (R = Yb, Y, Dy, Eu, Sm) are given in Figure 5b. The maximum value of f_i is 94.91% for the Y-O bond, indicating that the Y-O bond plays a dominated role in affecting the ε_r value of $Y_{2.95}R_{0.05}MgAl_3SiO_{12}$ ceramics.

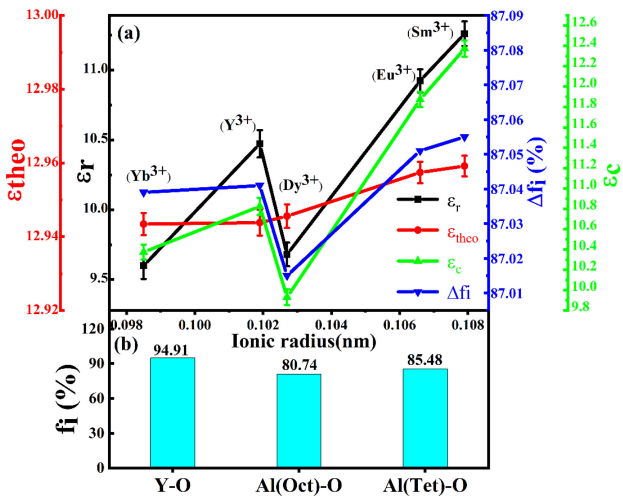

Figure 5. (**a**) ε_r, ε_{theo}, ε_c and Δf_i of $Y_{2.95}R_{0.05}MgAl_3SiO_{12}$ ceramics; (**b**) The average f_i of three types of bonds.

The lattice vibration of microwave dielectric ceramics has a great influence on dielectric loss. The lattice energy of the chemical bonds in microwave dielectric ceramics can be used to effectively evaluate the lattice vibration of ceramics [42]. Therefore, we can use the average lattice energy (U) value to predict the $Q \times f$ values, and the calculation results of the average lattice energy (U) value are listed in Table S2. The U, grain size, and $Q \times f$ values of the $Y_{2.95}R_{0.05}MgAl_3SiO_{12}$ ceramics are shown in Figure 6a. It can be seen that the U is consistent with the trend of $Q \times f$ values of $Y_{2.95}R_{0.05}MgAl_3SiO_{12}$ ceramics, suggesting that the U is an important factor affecting the $Q \times f$ values of $Y_{2.95}R_{0.05}MgAl_3SiO_{12}$ ceramics. Figure 6b shows U of the Y-O bonds, $Al_{(Oct)}$-O bonds, and $Al_{(Tet)}$-O bond in $Y_{2.95}R_{0.05}MgAl_3SiO_{12}$ ceramics ($Al_{(Tet)}$-O (33,533 kJ/mol)> Y-O(22,143 kJ/mol) > $Al_{(Oct)}$-O (21,989 kJ/mol)); it indicates that the $Al_{(Tet)}$-O bond plays a dominated role in determining the $Q \times f$ value. In addition, a larger average grain size shows fewer grain boundaries, which means higher $Q \times f$ values [43].

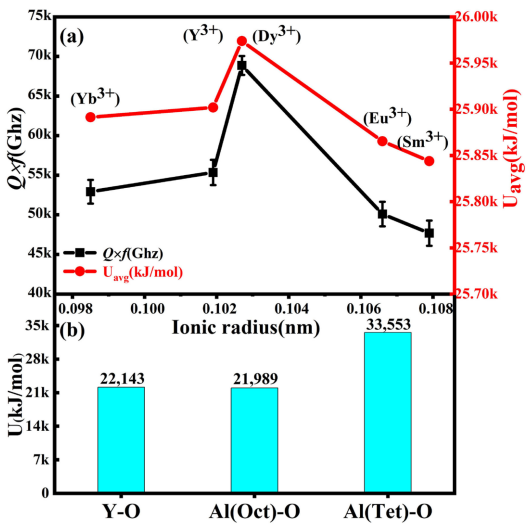

Figure 6. (**a**) $Q \times f$, average lattice energy, and average grain size of $Y_{2.95}R_{0.05}MgAl_3SiO_{12}$ ceramics; (**b**) The average U value of three types of bonds.

The τ_f is related to the bond valence (V_{ij}) and the bond energy (E). The E represents the strength of chemical bonds, which is generally evaluated by the amount of energy required to break the chemical bonds. The smaller the V_{ij}, the smaller the E required to recover the oxygen polyhedral deformation, leading to a decrease in the τ_f value. The V_{ij} value of $Y_{2.95}R_{0.05}MgAl_3SiO_{12}$ ceramics is calculated by Equations (7) and (8) [44,45]:

$$v_{ij} = exp\left\{\frac{R_{ij} - d_{ij}}{B}\right\} \tag{6}$$

$$V_{ij} = \sum_{j}^{i} v_{ij} \tag{7}$$

where R_{ij} is the bond valence parameter, B is a constant (0.37 Å), and d_{ij} is the bond length. The calculated results for E and V_{ij} are listed in Tables S3 and S4 (Supplementary Materials). The E, the V_{ij} of $Al_{(Tet)}$-O, and the τ_f value are shown in Figure 7a. It can be observed that the τ_f value of $Y_{2.95}R_{0.05}MgAl_3SiO_{12}$ ceramics fluctuates from −28.6 to −38.7 ppm/°C, which is consistent with the changing trend of average E and V_{ij}. Figure 6b shows the average E of Y-O, $Al_{(Oct)}$-O, and $Al_{(Tet)}$-O bonds ($Al_{(Tet)}$-O (307.28 kJ/mol) > $Al_{(Oct)}$-O (224.10 kJ/mol) > Y-O (218.47 kJ/mol)), which indicates that the $Al_{(Tet)}$-O bond plays a major role in the temperature stability of $Y_{2.95}R_{0.05}MgAl_3SiO_{12}$ ceramics.

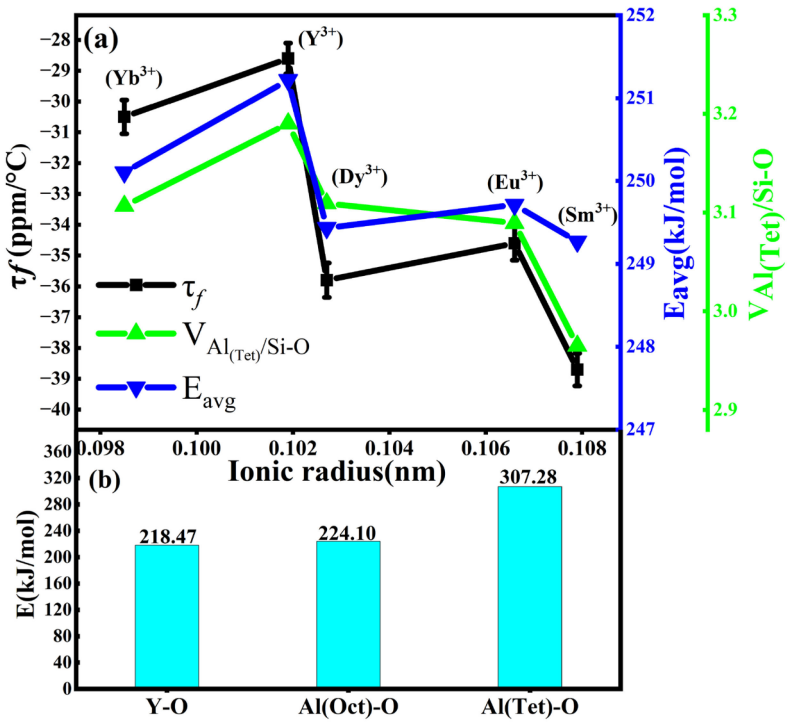

Figure 7. (**a**) The average E, bond valence of $V_{Al/Si-O}$, and τ_f value of $Y_{2.95}R_{0.05}MgAl_3SiO_{12}$ ceramic; (**b**) Average E of three types of bonds.

In order to further analyze the inherent microwave dielectric properties of $Y_{2.95}R_{0.05}MgAl_3SiO_{12}$ ceramics, the infrared reflectance spectrum was analyzed based on the classical harmonic oscillator model:

$$R(\omega) = \left|\frac{\sqrt{\varepsilon^*(\omega)} - 1}{\sqrt{\varepsilon^*(\omega)} + 1}\right|^2 \tag{8}$$

$$\varepsilon^*(\omega) = \varepsilon\prime(\omega) - i\varepsilon''(\omega) = \varepsilon_\infty + \sum_{j=1}^{n} \frac{S_j}{\omega_j^2 - \omega^2 + i\omega\gamma_j} \tag{9}$$

The relevant parameters in the formula were described in detail in the previous literature [46,47]. The infrared reflectance spectrum can be well-fitted with ten modes in Figure 8a. Table S5 (Supplementary Materials) lists the relevant phonon parameters. For $Y_{2.95}Dy_{0.05}MgAl_3SiO_{12}$ ceramics, the theoretical ε_r (~8.55) at 10.86 GHz in Figure 8b,c, is less than the measured value (~9.68). The calculated $Q \times f$ value is 89,752 GHz (f = 10.86 GHz, Q = 1/tanδ, and tanδ = 1.21 × 10^{-4}), which is greater than the measured value of 68,868 GHz. Differences between the measured and fitted values are because of the extrinsic loss affected by all kinds of defects [48].

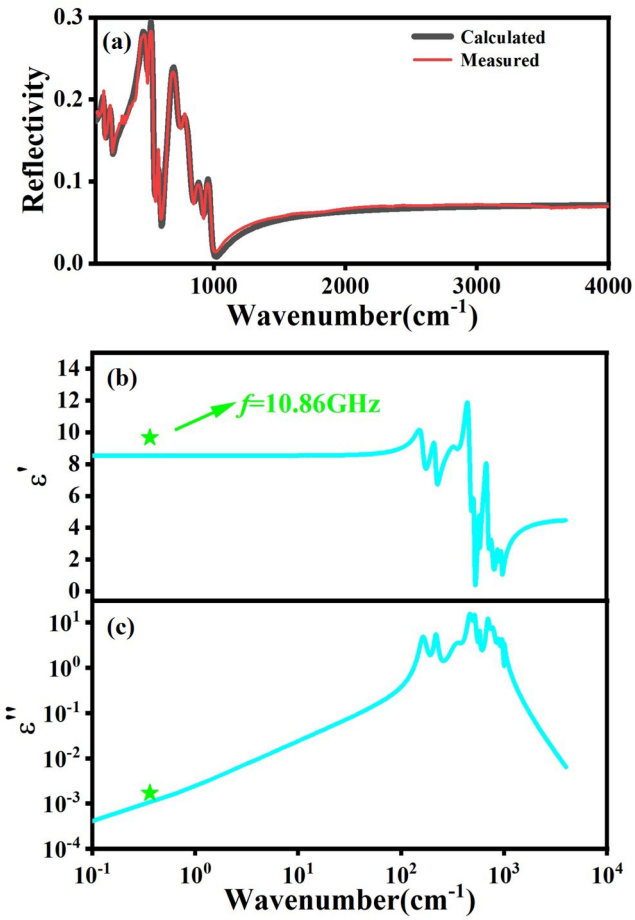

Figure 8. (**a**) Fitted and experimental infrared reflection spectrum of $Y_{2.95}Dy_{0.05}MgAl_3SiO_{12}$ ceramic and (**b**,**c**) fitted complex dielectric spectrum in the microwave region.

4. Conclusions

In this paper, the single-phase ceramics $Y_{2.95}R_{0.05}MgAl_3SiO_{12}$ (R = Yb, Y, Dy, Eu, Sm) were successfully prepared using a conventional ceramic sintering technology. The relationship between the crystal structure, microstructure, and microwave dielectric properties of $Y_{2.95}R_{0.05}MgAl_3SiO_{12}$ (R = Yb, Y, Dy, Eu, Sm) ceramics was analyzed by crystal structure refinement, SEM, bond valence theory, P–V–L theory, and infrared reflectance spectrum. The ε_r of $Y_{2.95}R_{0.05}MgAl_3SiO_{12}$ ceramics was mainly affected by the f_i of the Y-O bond. The τ_f value was mainly affected by the average E and bond valence of $Al_{(Tet)}$-O. In addition, infrared reflectance spectrum demonstrated that the calculated $Q \times f$ value was greater than the measured value, indicating the effect of extrinsic factors on the Q × f value. In particular, the microwave dielectric properties were obtained for $Y_{2.95}Dy_{0.05}MgAl_3SiO_{12}$, sintered at 1575 °C for 6 h, with ε_r = 9.68, $Q \times f$ = 68,866 GHz, and τ_f = −35.8 ppm/°C. The results show that $Y_{2.95}Dy_{0.05}MgAl_3SiO_{12}$ garnet ceramics have potential in 5G communication frequency bands, such as dielectric substrates, microstrip patch antenna, etc.

Supplementary Materials: The following supporting information can be downloaded at: https://www.mdpi.com/article/10.3390/cryst12111608/s1, Figure S1: Rietveld refinement results of $Y_{2.95}R_{0.05}MgAl_3SiO_{12}$(R = Yb, Y, Dy, Eu, Sm) ceramics (a) R = Yb; (b) R = Y; (c) R = Dy; (d)R = Eu; (e) R = Sm; (f) The crystal structure pattern of $Y_{2.95}R_{0.05}MgAl_3SiO_{12}$ ceramic.; Figure S2:The grain size distribution of each sample; Table S1: The bond ionicity f_i (%) of $Y_{2.95}R_{0.05}MgAl_3SiO_{12}$ ceramics.; Table S2: The lattice energy U (kJ/mol) of $Y_{2.95}R_{0.05}MgAl_3SiO_{12}$ ceramics; Table S3: The bond energy E (kJ/mol) of $Y_{2.95}R_{0.05}MgAl_3SiO_{12}$ ceramics; Table S4: The bond valence V_{ij} of $Y_{2.95}R_{0.05}MgAl_3SiO_{12}$ ceramics; Table S5: The Phonon parameters obtained from the fitting of the infrared reflectivity spectra of $Y_{2.95}Dy_{0.05}MgAl_3SiO_{12}$ ceramic.

Author Contributions: Conceptualization, Z.Y.; methodology, Z.Y. and G.W.; software, M.C.; validation, Y.J.; formal analysis, Z.X.; investigation, M.C.; resources, K.S.; data curation, Y.J. and G.W.; writing—original draft preparation, Y.J. and G.W.; writing—review and editing, D.W. and K.S.; visualization, B.Y. and K.S.; supervision, M.M. and K.S.; project administration, B.L. and K.S.; funding acquisition, K.S. and D.W. All authors have read and agreed to the published version of the manuscript.

Funding: This research was funded by [the Natural Science Foundation of China] grant number [52161145401], [51672063] and [the Guangdong Provincial Key Laboratory] grant number [2014B030301014].

Conflicts of Interest: The authors declare that they have no known competing financial interests or personal relationships that could have appeared to influence the work reported in this paper.

References

1. Du, C.; Zhou, D.; Li, R.T.; Chen, H.T.; Zhou, G.H.; Tang, B.; Darwish, M.A.; Xia, S.; Xu, Z. Fabrication of wideband low-profile dielectric patch antennas from temperature stable 0.65 $CaTiO_3$-0.35 $LaAlO_3$ microwave dielectric ceramic. *Adv. Electron. Mater.* **2022**, *8*, 2101414. [CrossRef]
2. Shen, G.X.; Che, W.Q.; Feng, W.J.; Shi, Y.R.; Xu, F.; Xue, Q. Ultra-low-loss millimeter-wave LTCC Bandpass filters based on flexible design of lumped and distributed circuits. *IEEE Trans. Circuits Syst. II Express Briefs* **2021**, *68*, 1123–1127. [CrossRef]
3. Wang, Z.J.; Pan, F.; Liu, L.L.; Du, Q.F.; Tang, R.T.; Ai, J.; Zhang, H.; Chen, Y. Enhanced microwave dielectric properties and sintering behaviors of Mg_2SiO_4-Li_2TiO_3-LiF ceramics by adding $CaTiO_3$ for LTCC and GPS antenna applications. *Crystals* **2022**, *12*, 512. [CrossRef]
4. Wong, S.W.; Chen, R.S.; Wang, K.; Chen, Z.N.; Chu, Q.X. U-shape slots structure on substrate integrated waveguide for 40-GHz bandpass filter using LTCC technology. *IEEE Trans. Compon. Packag. Manuf. Technol.* **2014**, *5*, 128–134. [CrossRef]
5. Wu, F.F.; Zhou, D.; Du, C.; Sun, S.K.; Pang, L.X. Temperature stable $Sm(Nb_{1-x}V_x)O_4$ ($0.0 < x < 0.9$) microwave dielectric ceramics with ultra-low dielectric loss for dielectric resonator antenna applications. *J. Mater. Chem. C* **2021**, *9*, 9962.
6. Xu, S.R.; Jiang, J.; Cheng, Z.L.; Chen, X.Y.; Sun, S.K.; Wang, D.W.; Zhang, T.J. Temperature stable, high-quality factor Li_2TiO_3-Li_4NbO_4 microwave dielectric ceramics. *Crystals* **2021**, *11*, 741. [CrossRef]
7. Du, C.; Fu, M.S.; Zhou, D.; Guo, H.H.; Chen, H.T.; Zhang, J.; Wang, J.P.; Wang, S.F.; Liu, H.W.; Liu, W.F.; et al. Dielectric resonator antenna with $Y_3Al_5O_{12}$ transparent dielectric ceramics for 5G millimeter-wave applications. *J. Am. Ceram. Soc.* **2021**, *104*, 4659–4668. [CrossRef]
8. Zhou, H.F.; Sun, W.D.; Liu, X.B. Microwave dielectric properties of $LiCa_3ZnV_3O_{12}$ and $NaCa_2Mg_2V_3O_{12}$ ceramics prepared by reaction-sintering. *Ceram. Int.* **2019**, *45*, 2629–2634. [CrossRef]
9. Tang, Y.; Li, H.; Li, J.; Fang, L. Relationship between Rattling Mg^{2+} ions and anomalous microwave dielectric behavior in $Ca_{3-x}Mg_{1+x}LiV_3O_{12}$ ceramics with garnet structure. *J. Am. Ceram. Soc.* **2021**, *41*, 7697–7702. [CrossRef]
10. Chen, J.; Tang, Y.; Xiang, H.; Fang, L. Microwave dielectric properties and infrared reflectivity spectra analysis of two novel low-firing $AgCa_2B_2V_3O_{12}$ (B=Mg, Zn) ceramics with garnet structure. *J. Am. Ceram. Soc.* **2018**, *38*, 670–4676. [CrossRef]
11. Rakhi, M.; Subodh, G. Crystal Structure and Microwave Dielectric Properties of $NaPb_2B_2V_3O_{12}$(B = Mg, Zn) Ceramics. *J. Am. Ceram. Soc.* **2018**, *38*, 4962–4966. [CrossRef]
12. Jin, W.; Yin, W.; Yu, S.; Tang, M.; Xu, T.; Kang, B.; Huang, H. Microwave dielectric properties of pure YAG transparent ceramics. *Mater. Lett.* **2016**, *173*, 47–49. [CrossRef]
13. Song, J.; Song, K.; Wei, J.; Lin, H.; Wu, J.; Xu, J.; Su, W.; Cheng, Z. Ionic occupation, structures, and microwave dielectric properties of $Y_3MgAl_3SiO_{12}$ garnet-type ceramics. *J. Am. Ceram. Soc.* **2018**, *101*, 244–251. [CrossRef]
14. Zhang, X.; Fan, G.; Lu, W.; Chen, Y.; Ruan, X. Effect of the spark plasma sintering parameters, LiF additive, and Nd dopant on the microwave dielectric and optical properties of transparent YAG ceramics. *J. Eur. Ceram. Soc.* **2018**, *36*, 2767–2772. [CrossRef]
15. Zhou, M.; Tang, B.; Xiong, Z.; Zhang, X.; Zhang, S. Effects of MgO doping on microwave dielectric properties of yttrium aluminum garnet ceramics. *J. Alloys Compd.* **2021**, *858*, 158139. [CrossRef]
16. Zhou, M.; Chen, H.; Zhang, X.; Tang, B. Phase composition, microstructure, and microwave dielectric properties of non-stoichiometric yttrium aluminum garnet ceramics. *J. Eur. Ceram. Soc.* **2022**, *42*, 472–477. [CrossRef]

17. Kim, J.C.; Kim, M.H.; Lim, J.B.; Nahm, S.; Paik, J.H.; Kim, J.H. Synthesis and Microwave Dielectric Properties of $Re_3Ga_5O_{12}$ (Re: Nd, Sm, Eu, Dy, Yb, and Y) Ceramics. *J. Am. Ceram. Soc.* **2007**, *90*, 641–644. [CrossRef]
18. Kim, J.C.; Kim, M.H.; Nahm, S.; Paik, J.H.; Kim, J.H.; Lee, H.J. Microwave dielectric properties of $Re_3Ga_5O_{12}$ (Re: Nd, Sm, Eu, Dy and Yb) ceramics and effect of TiO_2 on the microwave dielectric properties of $Sm_3Ga_5O_{12}$ ceramics. *J. Eur. Ceram. Soc.* **2007**, *27*, 2865–2870. [CrossRef]
19. Su, C.; Fang, L.; Ao, L.; Du, Q.; Zhai, Y.; Li, J.; Chen, J.; Tang, Y.; Liu, L. Correlation between crystal structure and microwave dielectric properties of two garnet-type ceramics in rare-earth-free gallates. *J. Eur. Ceram. Soc.* **2021**, *41*, 1962–1968. [CrossRef]
20. Su, C.; Ao, L.Y.; Zhai, Y.; Zhang, Z.W.; Tang, Y. Novel low-permittivity microwave dielectric ceramics in garnet-type $Ca_4ZrGe_3O_{12}$. *Mater. Lett.* **2020**, *275*, 128149. [CrossRef]
21. Zhai, Y.F.; Tang, Y.; Lia, J.; Duan, L. Structure, Raman spectra and properties of two low-ε_r microwave dielectric ceramics $Ca_3B_2Ge_3O_{12}$ (B = Al, Ga). *Ceram. Int.* **2020**, *46*, 28710–28715. [CrossRef]
22. Tang, Y.; Zhang, Z.W.; Li, J.; Xua, M.Y.; Zhai, Y.F. $A_3Y_2Ge_3O_{12}$ (A = Ca, Mg): Two novel microwave dielectric ceramics with contrasting τ_f and $Q\times f$. *J. Eur. Ceram. Soc.* **2020**, *40*, 3989–3995. [CrossRef]
23. Li, J.; Tang, Y.; Zhang, Z.W.; Fang, W.S.; Ao, L.Y.; Yang, A.H.; Liu, L.J.; Fang, L. Two novel garnet $Sr_3B_2Ge_3O_{12}$ (B = Yb, Ho) microwave dielectric ceramics with low permittivity and high Q. *J. Eur. Ceram. Soc.* **2021**, *41*, 1317–1323. [CrossRef]
24. Mei, H.R.; Zhang, L.B.; Li, C.C.; Rao, Z.G.; Shu, L.L. Compositional design, structure stability, and microwave dielectric properties in $Ca_3MgBGe_3O_{12}$ (B = Zr, Sn) garnet ceramics with tetravalent cations on B-site. *Ceram. Int.* **2022**, *48*, 4658–4664. [CrossRef]
25. Kagomiya, I.; Matsuda, Y.; Kakimoto, K. Microwave dielectric properties of YAG ceramics. *Ferroelectrics* **2009**, *387*, 1–6. [CrossRef]
26. Peng, S.; Zhao, C.G.; Huang, G.H.; Wang, S.J.; Xu, J.M.; Li, X.L.; Yu, S.Q. Crystal structure, sintering behavior and microwave dielectric properties of $Ca_xY_{3-x}Al_{5-x}Ti_xO_{12}$ ($0 \leq x \leq 2.0$) solid solution ceramics. *J. Mater. Sci. Mater. Electron.* **2018**, *29*, 17047–17053. [CrossRef]
27. Jiang, S.L.; Lu, T.; Chen, J. Ab initio study the effects of Si and Mg dopants on point defects and Y diffusion in YAG. *Comput. Mater. Sci.* **2013**, *69*, 261–266. [CrossRef]
28. Wu, G.F.; Ma, M.T.; Li, A.H. Crystal structure and microwave dielectric properties of Mg^{2+}-Si^{4+} co-modified yttrium aluminum garnet ceramics. *J. Mater. Sci. Mater. Electron.* **2022**, *33*, 4712–4720. [CrossRef]
29. Li, C.; Hou, J.L.; Ye, Y.J. Lattice occupying sites and microwave dielectric properties of Mg^{2+}-Si^{4+} co-doped $Mg_xY_{3-x}Al_{5-x}Si_xO_{12}$ garnet typed ceramics. *J. Mater. Sci. Mater. Electron.* **2022**, *33*, 2116–2124. [CrossRef]
30. Tan, Z.Y.; Song, K.X.; Liu, B.; Lin, H.X.; Wang, D.W. The effects of TiO_2 addition on microwave dielectric properties of $Y_3MgAl_3SiO_{12}$ ceramic for 5G application. *Ceram. Int.* **2020**, *46*, 15665–15669. [CrossRef]
31. Toby, B.H. EXPGUI, a graphical user interface for GSAS. *J. Appl. Crystallogr.* **2001**, *34*, 210–213. [CrossRef]
32. Rietveld, H.M. A profile refinement method for nuclear and magnetic structures. *J. Appl. Crystallogr.* **1969**, *2*, 65–71. [CrossRef]
33. Gu, Y.J.; Ding, X.B.; Hu, W.; Huang, J.L.; Li, Q.; Li, L.H.; Li, X.L.; Yang, X.H.; Chen, M.; Kim, B.H. Effect of Mg/B ratio and Sr^{2+} substitution for Mg^{2+} on the sintering, phase composition and microwave dielectric properties of $Mg_3B_2O_6$ ceramics. *Ceram. Int.* **2020**, *46*, 25888–25894. [CrossRef]
34. Wu, S.; Song, K.X.; Liu, P.; Lin, H.X.; Zhang, F.F.; Zheng, P.; Qin, H.B. Effect of TiO_2 doping on the structure and microwave dielectric properties of cordierite ceramics. *Am. Ceram. Soc.* **2015**, *98*, 1842–1847. [CrossRef]
35. Phillips, J.C. Dielectric definition of electronegativity. *Phys. Rev. Lett.* **1968**, *20*, 550–553. [CrossRef]
36. Phillips, J.C.; Vechten, J.A. Dielectric classification of crystal structures, ionization potentials, and band structures. *Phys. Rev. Lett.* **1969**, *22*, 705–708. [CrossRef]
37. Levine, B.F. Bond susceptibilities and ionicities in complex crystal structures. *J. Chem. Phys.* **1973**, *59*, 1463–1486. [CrossRef]
38. Wu, Z.J.; Meng, Q.B.; Zhang, S.Y. Semiempirical study on the valences of Cu and bond covalency in $Y_{1-x}Ca_xBa_2Cu_3O_{6+y}$. *Phys. Rev. B* **1998**, *58*, 958–962. [CrossRef]
39. Mahan, G. Octupole modifications of the Clausius-Mossotti relation. *Solid State Commun.* **1980**, *33*, 797–800. [CrossRef]
40. Shannon, R.D. Dielectric polarizabilities of ions in oxides and fluorides. *J. Appl. Phys.* **1993**, *73*, 348–366. [CrossRef]
41. Lou, W.; Song, K.; Hussain, F.; Liu, B.; Bafrooei, H.B.; Lin, H.; Su, W.; Shi, F.; Wang, D. Bond characteristics and microwave dielectric properties of $(Li_{0.5}Ga_{0.5})^{2+}$ doped $Mg_2Al_4Si_5O_{18}$ ceramics. *Ceram. Int.* **2020**, *46*, 28631–28638. [CrossRef]
42. Xiao, M.; He, S.S.; Lou, J.; Zhang, P. Structure and microwave dielectric properties of $MgZr(Nb_{1-x}Sb_x)_2O_8$ ($0 \leq x \leq 0.1$) ceramics. *J. Alloys Compd.* **2019**, *777*, 350–357. [CrossRef]
43. Penn, S.J.; Alford, N.M.; Templeton, A.; Wang, X.; Xu, M.; Reece, M.; Schrapel, K. Effect of porosity and grain size on the microwave dielectric properties of sintered alumina. *J. Am. Ceram. Soc.* **1997**, *80*, 1885–1888. [CrossRef]
44. Brese, N.; O'keeffe, M. Bond-valence parameters for solids. *Acta Crystallogr. Sect. B Struct. Sci.* **1991**, *47*, 192–197. [CrossRef]
45. Brown, I.D.; Altermatt, D. Bond-valence parameters obtained from a systematic analysis of the inorganic crystal structure database. *Acta Crystallogr. Sect. B Struct. Sci.* **1985**, *41*, 244–247. [CrossRef]
46. Xing, C.; Li, J.Z.; Wang, J.; Chen, H.L.; Qiao, H.Y.; Yin, X.Q.; Wang, Q.; Qi, Z.M.; Shi, F. Internal relations between crystal structures and intrinsic properties of nonstoichiometric $Ba_{1+x}MoO_4$ ceramics. *Inorg. Chem.* **2018**, *57*, 7121–7128. [CrossRef]
47. Lou, W.C.; Song, K.X.; Hussain, F. Microwave dielectric properties of $Mg_{1.8}R_{0.2}Al_4Si_5O_{18}$ (R = Mg, Ca, Sr, Ba, Mn, Co, Ni, Cu, Zn) cordierite ceramics and their application for 5G microstrip patch antenna. *J. Eur. Ceram. Soc.* **2022**, *42*, 2254–2260. [CrossRef]
48. Guo, D.; Zhou, D.; Li, W.B.; Pang, L.X.; Dai, Y.Z.; Qi, Z.M. Phase evolution, crystal structure, and microwave dielectric properties of water-insoluble (1-x)$LaNbO_4$-x$LaVO_4$($0 \leq x \leq 0.9$) ceramics. *Inorg. Chem.* **2017**, *56*, 9321–9329. [CrossRef]